Outage Performance of Mixed RF-FSO Cooperative Satellite-Aerial-Terrestrial Networks

1st Yuanyuan Ma
Beijing University of Posts and Telecommunications
Beijing, China
mayuan@bupt.edu.cn

2nd Tiejun Lv
Beijing University of Posts and Telecommunications
Beijing, China
lvtiejun@bupt.edu.cn

3rd Han Liu
Beijing Institute of Technology
Beijing, China
liuhan4335@bit.edu.cn

***Abstract*—This work investigates the secrecy outage performance of the uplink transmission of a radio-frequency -free-space optical cooperative satellite-aerial-terrestrial network. Specifically, the terrestrial source-to-aerial relay and the terrestrial source-to-eavesdroppers links with RF transmission experience independent and identical Nakagam-m fading, while the aerial relay-satellite receiver link with FSO transmission follows a unified Gamma-Gamma fading. Moreover, the cache-enabled aerial relay is with the most popular content caching scheme and a group of eavesdropping aerial terminals try to overhear the confidential information. Considering the randomness of satellite receiver, relay, and eavesdroppers, the secrecy outage performance of the cooperative uplink transmission in the considered satellite-aerial-terrestrial network is investigated and a closed-form analytical expression for the end-to-end secrecy outage probability is derived. Finally, Monte-Carlo simulations are shown to verify the accuracy of our analysis.**

***Index Terms*—RF-FSO system, satellite-aerial-terrestrial network, secrecy outage probability, uplink transmission, wireless caching**

I. Introduction

In recent years, free-space optical (FSO) communication has gained significant attention because of its license-free frequency spectrum, high security, and capacity [1], [2]. F-SO links have been presented as an ideal alternative to the conventional radio frequency (RF) links for secure satellite systems, because the laser beam has high directionality for security [3]. By utilizing relaying technology, the mixed RF-FSO systems combine both the advantages of the RF and FSO communication technologies [4]–[6].

Moreover, satellite communication is becoming an important enhancement of the six-generation (6G) systems to support the exponentially increasing data demand and variety of users across the world, since it can be widely applied in mass broadcasting, navigation, and disaster relief operations [7], [8] with high capability of seamless connectivity and wide coverage [9]–[12]. However, direct communication links between the satellite and the terrestrial terminals may not always be available, due to deep fading [13]. Thus, aerial relays have been regarded as an alternative and promising solution to extend and improve satellite-terrestrial communications [14]. The cooperative satellite-aerial-terrestrial network (SATN), which can effectively mitigate the impacts of deleterious masking effect in satellite links, has attracted a significant amount of attention [15]–[17]. The achievable secrecy-energy efficiency of the earth station under imperfect wiretap channel state information are maximized in the secure communication of rate-splitting multiple access based on the cognitive SATN in [15]. [16] derived the coverage probability of a dual-hop cooperative satellite-unmanned aerial vehicle communication system. The UAV trajectory and in-flight transmit power were jointly optimized by using a typical composite channel model including both large-scale and small-scale fading [17].

Furthermore, wireless caching [18] caching can be adopted into SATN caching. The outage probability (OP) of a cooperative SATN was evaluated in [19], considering the fundamental most popular content (MPC) and uniform content (UC) caching schemes at UAV relays. The OP and hit probability of the cache-enabled cooperate SATN were derived in [20], taking into account the uncertainty of the number and location of the aerial node. Compared to the UC scheme, the MPC scheme is widely used with a high hit rate.

Most of the authors of the aforementioned works focus on the downlink transmission performance of satellite-terrestrial/SATN systems, while the uplink transmission performance of cooperative SATN has not been extensively studied. On one hand, most of the data transmitted over the downlink are first received from the uplink and then delivered over the downlink, leading to a fact that the information security over the uplink is equally important and worth investigating. On the other hand, compared with the downlink transmission, there is a larger distribution space for the eavesdroppers in the uplink transmission scenarios, resulting in a tougher challenger to shield the information delivered over the uplink.

Motivated by these observations, in this work the secrecy outage performance of the uplink transmission in a mixed RF-FSO cooperative SATN is investigated. The main contributions of this paper are summarized as follows:

- We derived a closed-form expression for the lower bound of the secrecy OP (SOP) over terrestrial source–aerial relay (R) link considering the randomness of the positions of R and eavesdroppers;
- A closed-form expression for the OP over R-satellite receiver link is presented while considering that the satellite receiver is randomly distributed;
- The SOP of the considered SATN is investigated, while

978-3-903176-44-7 © 2022 IFIP

the cache-enabled relay adopts MPC caching scheme.

II. System Descriptions

A. System Model

Consider a mixed RF-FSO cooperative SATN, which consists of a terrestrial source (S), a cache-enabled aerial relay (R), a satellite receiver (D), and a group of aerial eavesdroppers ($E_k, 1 \leq k \leq K$). Specifically, the S-R and the S-Eves links with RF transmission experience independent and identical Nakagam-m fading, while the R-D link with FSO transmission follows a unified Gamma-Gamma fading. Here, R is equipped with $L \geq 2$ antennas and that maximum ratio combining (MRC) scheme is employed to process the received signals to achieve the maximum instantaneous signal-to-noise ratio (SNR), while each Eve is equipped with a single antenna for simplicity . Furthermore, the omnidirectional transmission antenna is assumed to be employed at S.

B. Channel Model

(1) S-R/Eve RF Link: The fading amplitudes of links $S \rightarrow R_l$, $S \rightarrow E_k$, which describe the channel fading between S and the l-th antenna of R, S and the l-th Eve, are denoted by h_q, where $q = \{SR_l, SE_k\}$. Consequently, the channel power $g_q = |h_q|^2$ are Gamma distributed with probability density function (PDF) and cumulative density function (CDF)

$$f_{g_q}(x) = \frac{\lambda_q^{m_q}}{\Gamma(m_q)} x^{m_q-1} \exp(-\lambda_q x) \tag{1}$$

and

$$F_{g_q} = \frac{\gamma(m_q, \lambda_q x)}{\Gamma(m_q)}, \tag{2}$$

respectively, where $\lambda_q = \frac{m_q}{\Omega_q}$, m_q and Ω_q denote the fading severity and the average channel power, respectively, $\Gamma(.)$ and $\gamma(.,.)$ are the Euler and the lower incomplete Gamma functions [21, Eq. (8.310.1)] and [21, Eq. (8.350.1)], respectively. For an integer m_q, (2) can be written as [21, Eq. (8.352.1)]

$$F_{g_q}(x) = 1 - \exp(-\lambda_q x) \sum_{k=0}^{m_q-1} \frac{\lambda_q^k x^k}{k!}. \tag{3}$$

We also assume that the channels between S and each antenna of R, channels between S and each Eve experience independent Nakagam-m fading. For simplicity, let m_R and Ω_R respectively denote the fading severity and the average channel power between S and each antenna of R, m_E and Ω_E respectively denote the fading severity and the average channel power between S and each Eve.

Meanwhile, when the MRC scheme is implemented at R, for a $(1, L)$ MRC system with a single transmit antenna and L receive antennas in Nakagam-m fading channels, the PDF and CDF of the combined channel power h_{SR} can be shown as [22]

$$f_{\|h_{SR}\|^2}(x) = \frac{\lambda_R^{Lm_R}}{\Gamma(Lm_R)} x^{Lm_R-1} \exp(-\lambda_R x) \tag{4}$$

and

$$F_{\|h_{SR}\|^2}(x) = \frac{\gamma(Lm_R, \lambda_R x)}{\Gamma(Lm_R)} = 1 - \exp(-\lambda_R x) \sum_{k=0}^{Lm_R-1} \frac{\lambda_R^k x^k}{k!}, \tag{5}$$

respectively, where $\lambda_R = \frac{m_R}{\Omega_R}$.

(2) R-D FSO Link: The PDF $f_{\gamma_D}(x)$ and CDF $F_{\gamma_D}(x)$ of the instantaneous SNR at D γ_D are given as [4]

$$f_{\gamma_D}(x) = Ax^{-1} G_{1,3}^{3,0}\left[Bx^{\frac{1}{r}} \middle| \begin{array}{c} \xi^2+1 \\ \xi^2, a, b \end{array}\right] \tag{6}$$

and

$$F_{\gamma_D}(x) = IG_{r+1,3r+1}^{3r,1}\left[\rho x \middle| \begin{array}{c} 1, K_1 \\ K_2, 0 \end{array}\right], \tag{7}$$

respectively, where $A = \frac{\xi^2}{r\Gamma(a)\Gamma(b)}$, $B = \frac{hab}{\sqrt[r]{\Omega_D}}$, $I = \frac{\xi^2 r^{a+b-2}}{(2\pi)^{r-1}\Gamma(a)\Gamma(b)}$, $\rho = \frac{(hab)^r}{\Omega_D r^{2r}}$, $K_1 = \Delta\left(r, \xi^2+1\right)$, $K_2 = \left[\Delta\left(r, \xi^2\right), \Delta(r, a), \Delta(r, b)\right]$, in which the parameters a and b are the severity of fading/scintillation due to the atmospheric turbulence conditions, r represents the detection scheme used at D, i.e. $r = 1$ for heterodyne detection (HD) and $r = 2$ for intensity modulation with direct detection (IM/DD), ξ is the ratio of the equivalent beam radius to the standard deviation of the pointing error displacement at the FSO receiver [5], Ω_D represents the average electrical SNR of the FSO link, $\Delta(k, a) = \frac{a}{k}, \frac{a+1}{k}, \cdots, \frac{a+k-1}{k}$, $h = \frac{\xi^2}{\xi^2+1}$, and $G_{g,q}^{m,n}[\cdot]$ is Meijer's G-function, as defined by [21, Eq. (9.301)].

C. Signal Model

The received signal at R and E_k can be given as

$$y_R(t) = \mathbf{h}_{SR}\sqrt{P_S d_R^{-\eta_1}} x_s(t) + n_R \tag{8}$$

and

$$y_{Ek}(t) = h_{SE}\sqrt{P_S d_{Ek}^{-\eta_1}} x_s(t) + n_E, \tag{9}$$

where $\mathbf{E}\left\{\left\|x_s(t)^2\right\|\right\} = 1$, P_S is the transmit power at S, $n_R \sim \mathcal{CN}(0, N_R)$ and $n_E \sim \mathcal{CN}(0, N_E)$ are the Gaussian noise at R and E, d_R and d_{Ek} denote the distance between S to R, S to the k-th E, respectively, η_1 is the path-loss factor.

Thus, the SNR at R and the strongest Eve E* are

$$\gamma_R = \frac{P_S \|\mathbf{h}_{SR}\|^2}{N_R d_R^{\eta_1}}, \tag{10}$$

and

$$\gamma_E = \frac{P_S \|h_{SE^*}\|^2}{N_E d_E^{\eta_1}}, \tag{11}$$

respectively, where h_{SE^*} is the channel fading between S and the strongest Eve, $d_E = \min\{d_{E1}, d_{E2}, \cdots, d_{EK}\}$.

When the pointing loss and scattering loss are not considered [23], the output electrical signal at D is

$$y_D(t) = \zeta\sqrt{\frac{P_R}{\mathcal{L}_{\text{FS}}}} \mathcal{L}_r I_{\text{fso}} x_r(t) + n_D(t), \tag{12}$$

where $\mathbf{E}\left\{\left\|x_r(t)^2\right\|\right\}=1$, P_R denotes the transmit power at R and ζ denotes the optical-to-electrical conversion coefficient, $\mathcal{L}_{\rm FS}=\left(\frac{4\pi f_c d_D}{c}\right)^2$ is the free space path loss, in which d_D is the distance between R and D, c is the velocity of light and f_c is the carrier wavelength of transmitted signal from R, while $\mathcal{L}_r$ includes transmitter gain, receiver gain, atmospheric attenuation, lenses losses, and system margin [23]. Besides, $I_{\rm fso}$ is the channel fading coefficient of the FSO link and $n_D(t)$ represents additive white Gaussian noise (AWGN) with zero mean and variance σ_d^2 at D. As a result, the SNR of the FSO link can be expressed as

$$\gamma_D=\frac{P_R\zeta^2\mathcal{L}_r^2 I_{\rm fso}^2}{\mathcal{L}_{\rm FS}\sigma_d^2}\overset{\Delta}{\cdot} \tag{13}$$

III. SOP Analysis for S-R Link

The secrecy capacity for S-R link in condition that R can successfully decode the signal x_s is defined as [24]

$$C_S=\max\left\{\log\left(1+\gamma_R\right)-\log\left(1+\gamma_E\right),0\right\}. \tag{14}$$

SOP in the first phase is the probability that the secrecy capacity is below a certain threshold (C_{th}), which is given by

$$\begin{aligned}\mathrm{SOP}_1&=\Pr\left\{\log\left(1+\gamma_R\right)-\log\left(1+\gamma_E\right)\le C_{th}\right\}\\&\ge\Pr\left\{\gamma_R\le\lambda\gamma_E\right\}=\mathrm{SOP}_1^{\rm L},\end{aligned} \tag{15}$$

where $\lambda=2^{C_{th}}$, $\mathrm{SOP}_1^{\rm L}$ is the lower bound of SOP_1. Here we assume that decoding threshold $\gamma_{\rm hold}<\lambda\gamma_E$.

Thus, $\mathrm{SOP}_1^{\rm L}$ can be presented as

$$\begin{aligned}\mathrm{SOP}_1^{\rm L}&\ge\Pr\left\{\frac{P_S\left\|\mathbf{h}_{SR}\right\|^2}{N_R d_R^{\eta_1}}\le\lambda\frac{P_S\left\|\mathbf{h}_{SE^*}\right\|^2}{N_E d_E^{\eta_1}}\right\}\\&=\Pr\left\{\left\|\mathbf{h}_{SR}\right\|^2\le N_R d_R^{\eta_1}\lambda\frac{\left\|\mathbf{h}_{SE^*}\right\|^2}{N_E d_E^{\eta_1}}\right\}.\end{aligned} \tag{16}$$

Let $X=\left\|\mathbf{h}_{SE^*}\right\|^2$, $Z=\frac{d_R^{\eta_1}}{d_E^{\eta_1}}$. $\mathrm{SOP}_1^{\rm L}$ can be obtained as

$$\begin{aligned}\mathrm{SOP}_1^{\rm L}&=\Pr\left\{\left\|\mathbf{h}_{SR}\right\|^2\le\frac{N_R}{N_E}\lambda XZ\right\}\\&=\int_{\frac{H_{\min}^{\eta_1}}{R_S^{\eta_1}}}^{\infty}\int_0^{\infty}F_{\left\|\mathbf{h}_{SR}\right\|^2}\left(\frac{N_R}{N_E}\lambda xz\right)f_X(x)\,dx f_Z(z)\,dz.\end{aligned} \tag{17}$$

Theorem 1. *The PDF of Z is expressed on the top of next page shown in* (18)*, where*

$$A_f=A_{1,f}+A_{2,f}, \tag{19}$$

$$B_{1,f}=\binom{K}{f}\frac{6\pi}{\eta_1 V_{S_1}}\frac{(-1)^{f+1}f}{R_S^{3f}}\frac{R_S^{3f+3}}{3f+3}, \tag{20}$$

$$B_{2,f}=-\binom{K}{f}\frac{6\pi}{\eta_1 V_{S_1}}\frac{(-1)^{f+1}f}{R_S^{3f}}\frac{H_{\min}R_S^{3f+2}}{3f+2}, \tag{21}$$

and

$$\begin{aligned}B_{3,f}=&\binom{K}{f}\frac{6\pi}{\eta_1 V_{S_1}}\frac{(-1)^{f+1}f}{R_S^{3f}}H_{\min}^{3f+3}\\&\times\left(\frac{f}{3f+3}-\frac{3f}{2\left(3f+2\right)}+\frac{1}{6}\right),\end{aligned} \tag{22}$$

in which $A_{1,f}$ and $A_{2,f}$ are presented as

$$\begin{aligned}A_{1,f}=&\binom{K}{f}\frac{\pi}{\eta_1 V_{S_1}}(-1)^{f+1}f\\&\times\left(2R_S^3-3H_{\min}R_S^2+H_{\min}^3\right),\end{aligned} \tag{23}$$

and

$$\begin{aligned}A_{2,f}=&\binom{K}{f}\frac{\pi}{\eta_1 V_{S_1}}(-1)^{f}\frac{f^2}{R_S^{3f}}\left[\frac{2}{f+1}R_S^{3f+3}\right.\\&-\frac{9}{3f+2}R_S^{3f+2}H_{\min}+\frac{1}{f}R_S^{3f}H_{\min}^3\\&\left.+\left(\frac{9}{3f+2}-\frac{2}{f+1}-\frac{1}{f}\right)H_{\min}^{3f+3}\right],\end{aligned} \tag{24}$$

respectively.

Proof: See Appendix A. ■

Theorem 2. *The lower bound of* SOP_1 *for S-R link of the considered RF-FSO cooperate HSAT can be derived as* (25) *shown on the top of next page, where $a_0=\lambda\lambda_R N_R/N_E$, the functions $H_1(\varrho,a,b,q,p)$ and $H_2(a,b,q,p)$ are expressed as*

$$\begin{aligned}&H_1\left(\varrho,a,b,q,p\right)\\&=\frac{\varrho^{p+1}\Gamma\left(q+1\right)}{\left(k-p\right)\left(\varrho b+a\right)^{q+1}}{}_2F_1\left(1,q+1;q-p+1;\frac{a}{\varrho b+a}\right)\\&\quad-\frac{\Gamma\left(q+1\right)}{\left(k-p\right)\left(b+a\right)^{q+1}}{}_2F_1\left(1,q+1;q-p+1;\frac{a}{b+a}\right)\end{aligned} \tag{26}$$

and

$$\begin{aligned}H_2\left(a,b,q,p\right)=&\frac{\Gamma\left(q+1\right)}{\left(k-p\right)\left(b+a\right)^{q+1}}\\&\times{}_2F_1\left(1,q+1;q-p+1;\frac{a}{b+a}\right),\end{aligned} \tag{27}$$

respectively, in which ${}_2F_1(\cdot,\cdot;\cdot;\cdot)$ denotes the hypergeometric function [21, Eq. (9.100)].

Proof: See Appendix B. ■

IV. Outage Analysis for R-D link

As FSO is adopted over R-D link, we assume that the information transmission from R to D will not be overheard by the eavesdroppers due to the highly directive and narrow nature of laser beam. We assume that D is uniformly distributed in the space, which is a part that the spherical cone with radius U_1 minus the one with radius U_2 (U_1 ¿ U_2. The two spherical cones are with same apex angle, $\Psi_{\rm D}$. we consider the case that the path-loss factor is 2 to simplify the analysis in the following. According to [13, Eq. (26)], the PDF of ${d_{\rm D}}^2$ is

$$f_{d_{\rm D}^2}=\tau\left[w_1^2\left(x\right)-w_2^2\left(x\right)\right], \tag{28}$$

$$f_Z(z)=\begin{cases}\sum_{f=1}^{K}A_f z^{-\frac{3f}{\eta_1}-1}, & \text{if } z>1;\\ \sum_{f=1}^{K}\left(B_{1,f}z^{\frac{3}{\eta_1}-1}+B_{2,f}z^{\frac{2}{\eta_1}-1}+B_{3,f}z^{-\frac{3f}{\eta_1}-1}\right), & \text{if } \frac{H_{\min}^{\eta_1}}{R_D^{\eta_1}}\le z\le 1;\\ 0, & \text{else}\end{cases} \tag{18}$$

$$\begin{aligned}\mathrm{SOP}_1^{\mathrm{L}}=&1-\lambda_E\sum_{k=0}^{L-1}\sum_{f=1}^{K}\frac{a_0^k}{k!}\left[B_{1,f}H_1\left(\rho,\lambda_E,a_0,k,k+\frac{3}{\eta_1}-1\right)+A_fH_2\left(\lambda_E,a_0,k,k-\frac{3f}{\eta_1}-1\right)\right.\\&\left.+B_{2,f}H_1\left(\rho,\lambda_E,a_0,k+,k+\frac{2}{\eta_1}-1\right)+B_{3,f}H_1\left(\rho,\lambda_E,a_0,k,k-\frac{3f}{\eta_1}-1\right)\right]\end{aligned} \tag{25}$$

where $w_1(x) = \min\{\mathrm{U}_1, H_R+\sqrt{x}\}$, $w_2(x) = \max\left\{\mathrm{U}_2, H_R\cos\Psi_{\mathrm{D}}+\sqrt{x-H_R^2\sin^2\Psi_{\mathrm{D}}}\right\}$, $\tau = \frac{3}{4H_R}\frac{1}{1-\cos\Psi_{\mathrm{D}}}\frac{1}{\mathrm{U}_1^3-\mathrm{U}_2^3}$, and the range of d_D^2 is $(\mathrm{U}_2-H_R)^2 = d_{D,\min}^2\le d_D^2\le d_{D,\max}^2 = \mathrm{U}_1^2+H_R^2-2\mathrm{U}_1H_R\cos\Psi_D$.

The OP of the link between R and D is $\mathrm{OP}_2 = \Pr\{\gamma_D<\gamma_{\mathrm{out}}\}$, where γ_{out} is the threshold that enables D to effectively receive the signals from R. When the height of R is unknown OP_2 is expressed as

$$\begin{aligned}\widetilde{\mathrm{OP}}_2 &= IG_{r+1,3r+1}^{3r,1}\left[\epsilon d_D^2\middle|\begin{array}{c}1,K_1\\K_2,0\end{array}\right]\\&=\int_{d_{D,\min}^2}^{d_{D,\max}^2} IG_{r+1,3r+1}^{3r,1}\left[\epsilon d_D^2\middle|\begin{array}{c}1,K_1\\K_2,0\end{array}\right]f_{d_D^2}(x)\,dx,\end{aligned} \tag{29}$$

where $\epsilon = \frac{(4\pi f_c)^2\sigma_d^2(hab)^r}{P_R c^2\zeta^2\mathcal{L}_r^2 r^{2r}}\gamma_{\mathrm{out}}$.

Employing Chebyshev-Gauss quadrature in the first case, the OP of the link between R and D can be finally written as (30) at the top of next page, where $b_1 = \frac{d_{D,\max}^2-d_{D,\min}^2}{2}$, $b_2 = \frac{d_{D,\max}^2+d_{D,\min}^2}{2}$, ω_i, x_i and N_{G} are the summation terms, weights, points of Gauss-Laguerre quadrature (GLQ) and summation number, respectively.

Corollary 1. *When the height of R is unknown, the approximation of* OP_2 *can be obtained by substituting* H_R, $d_{D,\min}^2$ *and* $d_{D,\max}^2$ *in their medians.*

Corollary 2. *The randomness of R have some effects on* SOP_1 *but have little effect on* OP_2 *owning to the huge gap between* H_R *and* R_S, *so* SOP_1 *and* OP_2 *are independent.*

V. SOP of the RF-FSO Cooperative SATN

With the limited storage capacity, R adopts the MPC caching scheme. It means only the most popular M files are stored at R, where M is the R's storage normalized by the size of each file. Especially, the total files number and the skewness parameter are N and α. Based on the analysis of outage in two phases of the considered system, the lower bound of SOP over the uplink of the RF-FSO cooperate SATN is

$$\mathrm{SOP} = \varphi\mathrm{OP}_2+\varphi'\left[1-(1-\mathrm{SOP}_1)(1-\mathrm{OP}_2)\right], \tag{31}$$

where $\varphi = \sum_{n=1}^{M}p_n$, $\varphi' = \sum_{n=M+1}^{N}p_n = 1-\varphi$, OP_2 is expressed as (30) in which $b_1 = \frac{\bar{d}_{D,\max}^2-\bar{d}_{D,\min}^2}{2}$, $b_2 = \frac{\bar{d}_{D,\max}^2+\bar{d}_{D,\min}^2}{2}$, and $\bar{d}_{D,\max}^2$, $\bar{d}_{D,\min}^2$ are the medians of $d_{D,\max}^2$, $d_{D,\min}^2$.

VI. Numerical Results and Discussion

In this section, Monte-Carlo simulation parameters are set as $\mathrm{U}_1 = 560$ km, $\mathrm{U}_2 = 535$ km, $R_S = 300$ m, $H_{\min} = 80$ m, $\Psi_D = \frac{\pi}{12}$, $R_{\mathrm{earth}} = 6371$ km, $a = 15.47$, $b = 14.6$, $\xi = 1.1$, $r = 2$, $\mathcal{L}_r = 81$ dB, $M = 10$, $\alpha = 1$, $N = 10^6$, $N_R = 1$ W, $N_E = 1$ W, $N_{\mathrm{G}} = 80$, $K = 3$, $L = 8$, $\lambda_R = 1.9$, $\lambda_E = 0.5$, $P_S = 10$ dBW, and $C_{th} = 0.01$ bits/s, $\zeta = 0.5$ [25].

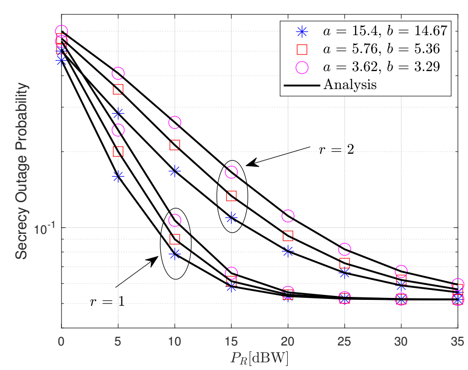

Fig. 1. SOP vs. P_R for various a, b and r.

Fig. 1 represents the SOP for different values (a,b) and r. One can also see that the SOP with the weakest turbulence $(a = 15.4, b = 14.67)$ is lower than that with strongest turbulence $(a = 3.62, b = 3.29)$. We know r represents the detection scheme used at D, where $r = 1$ is for HD and $r = 2$ is for IM/DD. By varying r and keeping (a,b) fixed in Fig. 1, the HD detection method can lead to better secrecy performance than IM/DD method. The reason for this is that the SNR obtained with the HD method is higher than that of IM/DD. Finally, SOP exhibits a floor because the secrecy capacity will become a constant, as reported in [26].

In Fig. 2, the size of the caching memory shows a positive influence on the SOP of the the considered system, since a large M means a large probability of taking no account of the

$$\begin{aligned}\widetilde{\mathrm{OP}}_2 &= \tau b_1 I \int_{-1}^{1} G_{r+1,3r+1}^{3r,1}\left[\epsilon\left(b_1 t+b_2\right)\middle|\begin{matrix}1, K_1\\ K_2, 0\end{matrix}\right]\left[w_1^2\left(b_1 t+b_2\right)-w_2^2\left(b_1 t+b_2\right)\right] dt \\ &= \tau b_1 I \sum_{i}^{N_{\mathrm{G}}} \omega_i G_{r+1,3r+1}^{3r,1}\left[\epsilon\left(b_1 x_i+b_2\right)\middle|\begin{matrix}1, K_1\\ K_2, 0\end{matrix}\right]\left[w_1^2\left(b_1 x_i+b_2\right)-w_2^2\left(b_1 x_i+b_2\right)\right]\end{aligned} \tag{30}$$

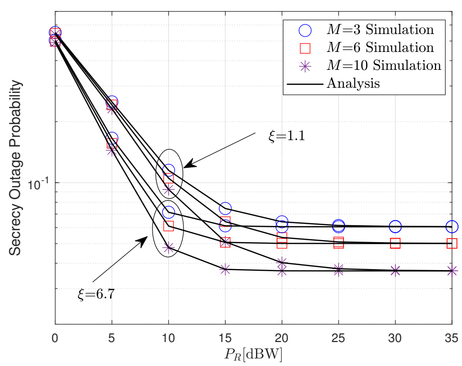

Fig. 2. SOP vs. P_R for various M and ξ.

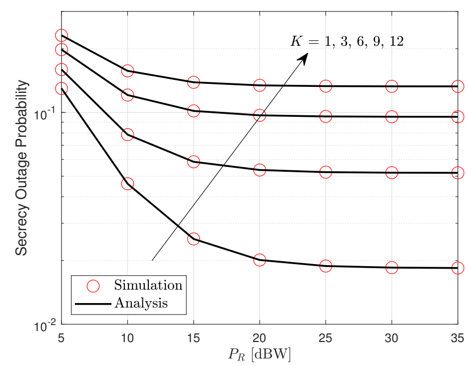

Fig. 4. SOP vs. P_R for various K.

terrestrial terminal-relay link. Moreover, the SOP with lower ξ is higher than that with larger ξ, because a larger ξ means high pointing accuracy over R-D link.

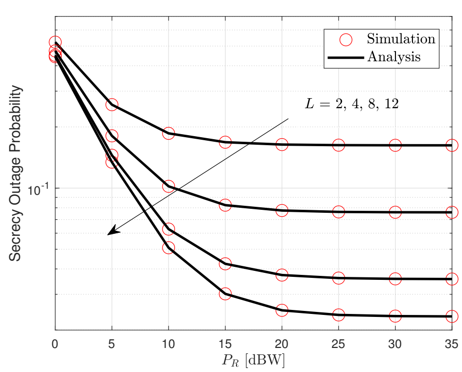

Fig. 3. SOP vs. P_R for various L.

The influence of the antenna number at R on the SOP performance is depicted in Fig. 3. As expected, L exhibits a positive effect. A large L results in a small SOP, meaning better secrecy performance, since a large L can bring large diversity gain at R.

Fig. 4 presents the SOP performance for various K, while P_R increasing. Obviously, K shows a negative impact on the SOP performance, as a large K means that Eves are distributed around terrestrial terminals more densely. This explains that SOP degrades when the number of Eves increases.

VII. Conclusions

We have investigated the SOP of the uplink transmission of a mixed RF-FSO cooperative SATN in the presence of a group of aerial Eves. Considering the randomness of R, D, and Eves, and employing stochastic geometry, the secrecy outage performance of the cooperative uplink transmission in the considered SATN has been investigated and the closed-form expression for the end-to-end SOP has been derived. Simulations confirm the analytical results.

Appendix A

The coordinate of R can be presented as (r_R, θ_R, ψ_R), where $H_{\min} \le r_R \le R_S$, $0 \le \theta_R \le \arccos\frac{H_{\min}}{R_S}$ and $0 \le \psi_R \le 2\pi$. Employing Lemma 4 of [13], the CDF of the distance between S and R, $d_R = r_R$, is

$$F_{d_R}(x) = \frac{\pi}{3V_{S_1}}\left(2x^3 - 3H_{\min}x^2 + H_{\min}^3\right), \tag{32}$$

where $V_{S_1} = \frac{\pi}{3}\left(2R_S^3 - 3H_{\min}R_S^2 + H_{\min}^3\right)$ and R_S is the coverage space radius of S.

The CDF and the PDF of d_E are [27]

$$F_{d_E}(d_E) = 1 - \left(1 - \frac{d_E^3}{R_S^3}\right)^K \tag{33}$$

and

$$f_{d_E}(d_E) = \frac{\partial F_{d_E}(d_E)}{\partial d_E} = K\left(1 - \frac{d_E^3}{R_S^3}\right)^{K-1}\frac{3{d_E}^2}{R_S^3}, \tag{34}$$

respectively, where $0 \le d_E \le R_S$.

Thus, $f_{d_R^{\eta_1}}$ and $f_{d_E^{\eta_1}}(x)$ are derived.

If $Z = \frac{d_R^{\eta_1}}{d_E^{\eta_1}} \le 1$, the CDF of Z is

$$F_Z(z) = \int_{H_{\min}^{\eta_1}/z}^{R_S^{\eta_1}} \int_{H_{\min}^{\eta_1}/y}^{z} H_Z(y,u), \tag{35}$$

where

$$H_{\mathrm{Z}}\left(y,u\right)=\frac{2\pi y}{\eta_1 V_{S_1}}\left(\left(yu\right)^{\frac{3}{\eta_1}-1}-H_{\min}\left(yu\right)^{\frac{2}{\eta_1}-1}\right)\times\sum_{f=1}^{K}\binom{K}{f}\left(-1\right)^{f+1}\frac{3f}{\eta_1 R_S^{3f}}y^{\frac{3f}{\eta_1}-1}dudy. \tag{36}$$

Using polynomial integration and differentiation, the PDF of Z is obtained as (18).

APPENDIX B

Substituting the CDF of $\left\|\mathbf{h}_{SR}\right\|^2$, $\mathrm{SOP}_1^{\mathrm{L}}$ is expressed as

$$\mathrm{SOP}_1^{\mathrm{L}}=1-\sum_{k=0}^{L-1}\frac{\left(a_0\right)^k}{k!}\int_{\rho}^{\infty}\int_{0}^{\infty}\exp\left(-a_0 xz\right)\times x^k z^k f_X\left(x\right)dx f_Z\left(z\right)dz, \tag{37}$$

where $a_0=\lambda\lambda_R\frac{N_R}{N_E}$ and $\rho=\frac{H_{\min}^{\eta_1}}{R_S^{\eta_1}}$.

Changing the range of integration and substituting the PDF of $\left\|\mathbf{h}_{SE^*}\right\|^2$ and $\frac{d_R^{\eta_1}}{d_E^{\eta_1}}$, there exists

$$H\left(\varrho,a,b,q,p\right)=\int_{0}^{\infty}\int_{\rho}^{\infty}\exp\left(-ax\right)\times x^q\exp\left(-bxz\right)z^p dxdz. \tag{38}$$

Using [28, Eq. (8.19.25)], $H\left(\varrho,a,b,q,p\right)$ is derived as

$$H\left(\varrho,a,b,q,p\right)=\frac{\varrho^{p+1}\Gamma\left(q+1\right)}{\left(k-p\right)\left(\varrho b+a\right)^{q+1}}\times{}_2F_1\left(1,q+1;q-p+1;\frac{a}{\varrho b+a}\right). \tag{39}$$

Thus, $\mathrm{SOP}_1^{\mathrm{L}}$ is derived.

REFERENCES

[1] L. Han, Y. Wang, X. Liu, and B. Li, "Secrecy performance of FSO using HD and IM/DD detection technique over F-distribution turbulence channel with pointing error," *IEEE Wireless Commun. Lett.*, vol. 10, no. 10, pp. 2245–2248, 2021.

[2] R. Singh, M. Rawat, and A. Jaiswal, "On the physical layer security of mixed FSO-RF SWIPT system with non-ideal power amplifier," *IEEE Photon.J.*, vol. 13, no. 4, pp. 1–17, 2021.

[3] H. Lei, H. Luo, K.-H. Park, Z. Ren, G. Pan, and M.-S. Alouini, "Secrecy outage analysis of mixed RF-FSO systems with channel imperfection," *IEEE Photon. J.*, vol. 10, no. 3, pp. 1–13, 2018, Art no. 7904113.

[4] H. Lei, Z. Dai, K.-H. Park, W. Lei, G. Pan, and M.-S. Alouini, "Secrecy outage analysis of mixed RF-FSO downlink SWIPT systems." *IEEE Trans. Commun.*, vol. 66, no. 12, pp. 6384–6395, 2018.

[5] E. Zedini, H. Soury, and M.-S. Alouini, "On the performance analysis of dual-hop mixed FSO/RF systems," *IEEE Trans. Wireless Commun.*, vol. 15, no. 5, pp. 3679–3689, 2016.

[6] E. Soleimani-Nasab and M. Uysal, "Generalized performance analysis of mixed RF/FSO cooperative systems," *IEEE Trans. Wireless Commun.*, vol. 15, no. 1, pp. 714–727, 2016.

[7] C. D. Alwis, A. Kalla, Q.-V. Pham, P. Kumar, K. Dev, W.-J. Hwang, and M. Liyanage, "Survey on 6G frontiers: Trends, applications, requirements, technologies and future research," *IEEE Open J. Commun. Soc.*, vol. 2, pp. 836–886, 2021.

[8] H. Tataria, M. Shafi, A. F. Molisch, M. Dohler, H. Sjöland, and F. Tufvesson, "6G wireless systems: Vision, requirements, challenges, insights, and opportunities," *Proc. IEEE*, vol. 109, no. 7, pp. 1166–1199, 2021.

[9] Z. Lin, M. Lin, W.-P. Zhu, J.-B. Wang, and J. Cheng, "Robust secure beamforming for wireless powered cognitive satellite-terrestrial networks," *IEEE Trans. Cogn. Commun. Netw.*, vol. 7, no. 2, pp. 567–580, 2021.

[10] X. Zhang, D. Guo, K. An, G. Zheng, S. Chatzinotas, and B. Zhang, "Auction-based multichannel cooperative spectrum sharing in hybrid satellite-terrestrial IoT networks," *IEEE Internet of Things Journal*, vol. 8, no. 8, pp. 7009–7023, 2021.

[11] X. Zhang, K. An, B. Zhang, Z. Chen, Y. Yan, and D. Guo, "Vickrey auction-based secondary relay selection in cognitive hybrid satellite-terrestrial overlay networks with non-orthogonal multiple access," *IEEE Wireless Communications Letters*, vol. 9, no. 5, pp. 628–632, 2020.

[12] X. Zhang, B. Zhang, K. An, B. Zhao, Y. Jia, Z. Chen, and D. Guo, "On the performance of hybrid satellite-terrestrial content delivery networks with non-orthogonal multiple access," *IEEE Wireless Communications Letters*, vol. 10, no. 3, pp. 454–458, 2021.

[13] G. Pan, J. Ye, Y. Zhang, and M.-S. Alouini, "Performance analysis and optimization of cooperative satellite-aerial-terrestrial systems," *IEEE Trans. Wireless Commun.*, vol. 19, no. 10, pp. 6693–6707, 2020.

[14] T. Li, J. Ye, J. Dai, H. Lei, W. Yang, G. Pan, and Y. Chen, "Secure UAV-to-vehicle communications," *IEEE Trans. Commun.*, vol. 69, no. 8, pp. 5381–5393, 2021.

[15] Z. Lin, M. Lin, B. Champagne, W.-P. Zhu, and N. Al-Dhahir, "Secure and energy efficient transmission for RSMA-based cognitive satellite-terrestrial networks," *IEEE Wireless Commun. Lett.*, vol. 10, no. 2, pp. 251–255, 2021.

[16] Y. Tian, G. Pan, M. A. Kishk, and M.-S. Alouini, "Stochastic analysis of cooperative satellite-UAV communications," *IEEE Trans. Wireless Commun.*, pp. 1–1, 2021.

[17] X. Li, W. Feng, Y. Chen, C.-X. Wang, and N. Ge, "Maritime coverage enhancement using UAVs coordinated with hybrid satellite-terrestrial networks," *IEEE Trans. Commun.*, vol. 68, no. 4, pp. 2355–2369, 2020.

[18] Z. Chen, J. Lee, T. Q. S. Quek, and M. Kountouris, "Cooperative caching and transmission design in cluster-centric small cell networks," *IEEE Trans. Wireless Commun.*, vol. 16, no. 5, pp. 3401–3415, 2017.

[19] P. K. Sharma, D. Gupta, and D. I. Kim, "Outage performance of 3D mobile UAV caching for hybrid satellite-terrestrial networks," *IEEE Trans. Veh. Techno*, vol. 70, no. 8, pp. 8280–8285, 2021.

[20] X. Zhang, B. Zhang, K. An, G. Zheng, S. Chatzinotas, and D. Guo, "Stochastic geometry-based analysis of cache-enabled hybrid satellite-aerial-terrestrial networks with non-orthogonal multiple access," *IEEE Trans. Wireless Commun.*, pp. 1–1, 2021, doi=10.1109/TWC.2021.3103499.

[21] I. S. Gradshteyn and I. M. Ryzhik, *Table of Integrals, Series, and Products*, 7th ed. Elsevier/Academic Press, Amsterdam, 2007.

[22] E. Al-Hussaini and A. Al-Bassiouni, "Performance of MRC diversity systems for the detection of signals with Nakagami fading," *IEEE Trans. Commun.*, vol. 33, no. 12, pp. 1315–1319, 1985.

[23] H. Kong, M. Lin, W.-P. Zhu, H. Amindavar, and M.-S. Alouini, "Multiuser scheduling for asymmetric FSO/RF links in satellite-UAV-terrestrial networks," *IEEE Wireless Commun. Lett.*, vol. 9, no. 8, pp. 1235–1239, 2020.

[24] M. Bloch, J. Barros, M. R. D. Rodrigues, and S. W. McLaughlin, "Wireless information-theoretic security," *IEEE Trans. Inf. Theory*, vol. 54, no. 6, pp. 2515–2534, 2008.

[25] J.-Y. Wang, J.-B. Wang, M. Chen, N. Huang, L. Jia, and R. Guan, "Ergodic capacity and outage capacity analysis for multiple-input single-output free-space optical communications over composite channels," *Opt. Eng.*, vol. 53(1) 016107, 2014.

[26] H. Lei, I. S. Ansari, G. Pan, B. Alomair, and M.-S. Alouini, "Secrecy capacity analysis over $\alpha-\mu$ fading channels," *IEEE Commun. Lett.*, vol. 21, no. 6, pp. 1445–1448, 2017.

[27] M. Erdelj, E. Natalizio, K. R. Chowdhury, and I. F. Akyildiz, "Help from the sky: Leveraging UAVs for disaster management," *IEEE Pervasive Comput.*, vol. 16, no. 1, pp. 24–32, 2017.

[28] "*NIST Digital Library of Mathematical Functions*," Release 1.1.3 of 2021-09-15, F. W. J. Olver, A. B. Olde Daalhuis, D. W. Lozier, B. I. Schneider, R. F. Boisvert, C. W. Clark, B. R. Miller, B. V. Saunders, H. S. Cohl, and M. A. McClain, eds.